Transverse coupling to the core of a photonic crystal fiber: the photo-inscription of gratings

Graham D. Marshall[1], Dougal J. Kan[2], Ara A. Asatryan[2],
Lindsay C. Botten[2], and Michael J. Withford[1]

[1]*Centre for Ultrahigh bandwidth Devices for Optical Systems, Centre for Lasers and Applications,
Macquarie University, Sydney, NSW 2109, Australia*
[2]*Centre for Ultrahigh bandwidth Devices for Optical Systems, Department of Mathematical Sciences, University of
Technology Sydney, Sydney, NSW 2007, Australia*
graham@ics.mq.edu.au

http://www.cudos.org.au

Abstract: The effect of the microstructure on transversely coupled laser light into the core of a photonic crystal fiber is investigated. Computational two-dimensional modeling and direct experimental measurements indicate that there exist angles and positions of the fiber microstructure, relative to a transversely launched laser beam, that preferentially couple laser light into the fiber core. The implications of these observations on long period and fiber-Bragg grating fabrication in photonic crystal fibers are discussed.

©2007 Optical Society of America

OCIS codes: (060.2340) Fiber optics components; (230.1480) Bragg reflectors; (080.2720) Geometrical optics, mathematical methods; (290.4210) Multiple scattering.

References and links

1. Y. F. Li, F. C. Salisbury, Z. M. Zhu, T. G. Brown, P. S. Westbrook, K. S. Feder, and R. S. Windeler, "Interaction of supercontinuum and Raman solitons with microstructure fiber gratings," Opt. Express 13, 998-1007 (2005).
2. B. J. Eggleton, C. Kerbage, P. S. Westbrook, R. S. Windeler, and A. Hale, "Microstructured optical fiber devices," Opt. Express 9, 698-713 (2001).
3. H. Dobb, K. Kalli, and D. J. Webb, "Temperature-insensitive long period grating sensors in photonic crystal fibre," Electron. Lett. 40, 657-658 (2004).
4. B. J. Eggleton, P. S. Westbrook, R. S. Windeler, S. Spalter, and T. A. Strasser, "Grating resonances in air-silica microstructured optical fibers," Opt. Letters 24, 1460-1462 (1999).
5. V. Beugin, L. Bigot, P. May, M. Lancry, Y. Quiquempois, M. Douay, G. Melin, A. Fleureau, S. Lempereur, and L. Gasca, "Efficient Bragg gratings in phosphosilicate and germanosilicate photonic crystal fiber," Appl. Opt. 45, 8186-8193 (2006).
6. N. Groothoff, J. Canning, E. Buckley, K. Lyttikainen, and J. Zagari, "Bragg gratings in air-silica structured fibers," Opt. Lett. 28, 233-235 (2003).
7. L. B. Fu, G. D. Marshall, J. A. Bolger, P. Steinvurzel, E. C. Magi, M. J. Withford, and B. J. Eggleton, "Femtosecond laser writing Bragg gratings in pure silica photonic crystal fibres," Electron. Lett. 41, 638-640 (2005).
8. H. R. Sorensen, J. Canning, J. Laegsgaard, K. Hansen, and P. Varming, "Liquid filling of photonic crystal fibres for grating writing," Opt. Commun. 270, 207-210 (2007).
9. S. J. Mihailov, D. Grobnic, H. M. Ding, C. W. Smelser, and J. Broeng, "Femtosecond IR laser fabrication of Bragg gratings in photonic crystal fibers and tapers," IEEE Photon. Technol. Lett. 18, 1837-1839 (2006).
10. G. Brambilla, A. A. Fotiadi, S. A. Slattery, and D. N. Nikogosyan, "Two-photon photochemical long-period grating fabrication in pure-fused-silica photonic crystal fiber," Opt. Lett. 31, 2675-2677 (2006).
11. P. Steinvurzel, E. D. Moore, E. C. Magi, B. T. Kuhlmey, and B. J. Eggleton, "Long period grating resonances in photonic bandgap fiber," Opt. Express 14, 3007-3014 (2006).
12. S. O. Kucheyev and S. G. Demos, "Optical defects produced in fused silica during laser-induced breakdown," Appl. Phys. Lett., 82, 3230-3232 (2003).
13. T. P. White, B. T. Kuhlmey, R. C. McPhedran, D. Maystre, G. Renversez, C. M. de Sterke, and L. C. Botten, "Multipole method for microstructured optical fibers. I. Formulation," JOSA B-Opt. Phys. 19, 2322-2330 (2002).
14. B. T. Kuhlmey, T. P. White, G. Renversez, D. Maystre, L. C. Botten, C. M. de Sterke, and R. C. McPhedran, "Multipole method for microstructured optical fibers. II. Implementation and results," J.Opt. Soc. Am. B 19, 2331-2340 (2002).

15. D. N. Nikogosyan, "Multi-photon high-excitation-energy approach to fibre grating inscription," Meas. Sci. Tech., 18, R1-R29 (2007).

1. Introduction

Photonic crystal fibers (PCFs) that employ a lattice of air holes in their cladding region are of great interest to many fields in fiber-based photonics. The unique bandgap properties of the air-cladding region allow manipulation of the modal, linear and non-linear characteristics of the fiber. Furthermore it is often desirable to incorporate Bragg and long-period grating structures in air-clad PCFs in order to increase the functionality of the fiber. Photonic crystal fibers incorporating gratings have been investigated in supercontinuum generation [1], in studies of mode propagation in PCFs [2], and in fiber based sensors [3]. Fabricating a grating in a PCF presents a number of technical challenges since the photosensitivity of the commonly used pure silica fibers is low and the lattice of air holes impedes transverse coupling of light into the core. It is in this transverse direction, through the strongly scattering air-cladding region, that optically induced grating inscription techniques seek to access the core.

Previous reports of fiber-Bragg grating (FBG) structures written using a conventional cylindrical lens and phase-mask technique in PCF have addressed the scattering effect of the cladding through a number of means. These include the use of custom manufactured fibers with doped cores that are photosensitive [4, 5], prolonged fiber exposure times [6, 7], filling the scattering holes with a refractive index matching fluid [8], tapering of the PCF leading to a collapse of the air-holed region to provide direct optical access to the fiber core [9], and scanning the laser focus over the microstructured region in order to exploit all possible scattering paths to the core [9]. In some of these studies the PCF was hydrogen or deuterium loaded to exploit this well documented technique of increasing the photosensitivity of pure silica and doped glasses to ultraviolet light.

The fabrication of long period gratings (LPGs) in PCF has been somewhat more successful than the production of fiber-Bragg gratings. Several techniques have been reported and include laser exposure using spherical focusing geometries [10], electric arc exposure [3], and the application of mechanical stress [11]. The latter two techniques modify the physical form of the PCF and thereby circumvent the requirement of optical access to the fiber core. The results presented in this paper (which concern cylindrical focusing) are also pertinent to spherical focusing geometries. However, we do not present a solution to the spherical problem here and this is a topic for further investigation.

In the majority of cases where gratings are to be permanently inscribed in PCF, the core of the fiber is exposed to a laser as a means of modifying the local refractive index. Yet despite the growing interest in this field, there has been no rigorous study into the effect of the air-silica holed region on the passage of a writing laser beam focused through the cladding at the fiber core. In this paper, we present experimental and theoretical modeling studies that directly illustrate the transmission through cladding to core (hereafter called transverse coupling) effect in a typical PCF at two different wavelengths. The problem is tackled in an essentially two-dimensional (2D) manner, given that the motivation for this work was to study the cylindrical focusing geometry used in a phase mask based FBG writing setup. Besides being the most common method for writing FBGs this approach also lends itself well to computational studies where a 2D model can be used.

2. Experimental study

The PCF used in this study was an endlessly single mode fiber (ESM) from Crystal Fibre (A/S part number ESM-12-01). This fiber was selected due to its popularity in both Bragg and long period grating writing applications. The fiber had a core diameter of 12.0 μm, a hole pitch of 8.0 μm and a typical hole diameter of 3.7 μm. The fiber has a nominal cladding diameter of 125 μm and is composed entirely of pure fused silica. Three layers of air-holes surround the fiber core. An optical micrograph of the fiber cross-section is shown in Fig. 1.
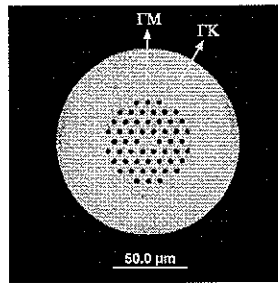
Fig. 1. Optical micrograph of ESM-12-01 with the ΓM and ΓK directions labeled.

In order to study the transverse coupling of laser light into the PCF under investigation, a suitable metric for the amount of laser light intersecting the core was required. It was not desirable to use FBG grating growth rates as this metric because exposure times were expected to be lengthy and many angles would be required to explore the required parameter space. Indeed, a more immediate and deterministic metric was sought. This was found in the 1.9 eV photoluminescence band, observed when fused silica is exposed to UV laser light [12]. Under exposure to UV laser light, the fused silica optical fiber used in this study was observed to emit this characteristically red luminescence. When the laser beam was focused on the optical fiber such that coupling to the core was achieved, this red luminescence could be observed emanating from the fiber after being core guided from the exposed region to the cleaved end facet. This luminescence was imaged and measured using a microscope objective coupled to a beam profiling CCD camera and computer. Photoluminescence created in the regions outside of the core, including the air-cladding region, was lost from the fiber through coupling into the polymer jacket.

The experimental setup used to make measurements of the PCF transverse coupling is shown in Fig. 2. The optical fiber under test was held in a computer controlled rotating fiber mount (ROT). After leaving the rotating fiber mount, the fiber was held between two fiber capillaries (FC) that precisely determined the position of the fiber. These capillaries held the fiber such that it could rotate with ease whilst not moving laterally. The movement of the fiber when held in this manner was below the observable limit when using the microscope objective and CCD camera as a vision system and was expected to be less than 0.5 μm. The fiber was locally stripped of its polymer jacket where it was exposed to the linearly polarized 267 nm laser light (3rd harmonic generated from 120 fs pulses at 800 nm, from a Spectra-Physics Hurricane). A 104 mm focal length fused silica cylindrical lens was used to focus the laser; the laser beam radius was 2.2 mm at the $1/e^2$ point before focusing, giving an expected minimum waist at the focus of 4.0 μm. The cylindrical lens could be adjusted in the vertical, longitudinal and center rotation directions in order to overlap the laser focus with the fiber core.

The fiber luminescence detection system comprised a Mitutoyo 100× Plan Apochromat 0.7 NA microscope objective coupled to a Pulnix TM-745 CCD camera. The camera was used with a 12 bit digitizing frame grabbing card and beam profiling software (from Spiricon Inc.) to measure the luminescence signal emanating from the core. To study the effects of different linear polarizations on the transverse coupling, a half-wave plate (not shown in Fig. 2) could be inserted into the incident laser beam in front of the cylindrical lens. The use of the computer controlled rotation stage and beam profiling software enabled the automated collection of the PL signal with rotational angle; a full 360° rotational scan with 1 increments took approximately 20 minutes to complete.
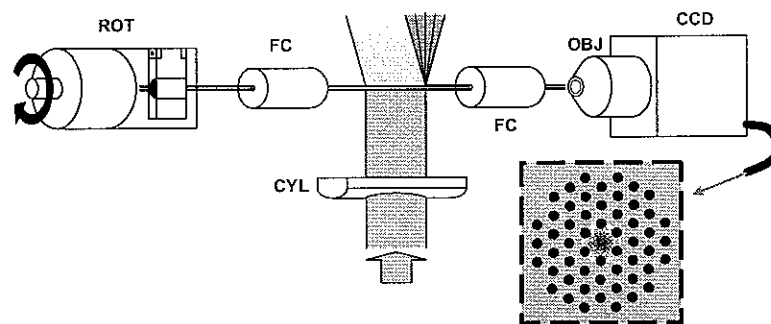
Fig. 2. Schematic of the optical fiber arrangement and photoluminescence detection system. The PCF is attached to a computer controlled 360° rotation stage (ROT) before passing through two fiber capillaries (FC) that prevent translation of the fiber while allowing rotation. The fiber luminescence is imaged by a microscope objective (OBJ) on to a CCD camera (CCD). A cylindrical lens (CYL) focuses the incident laser beam (in grey) on the PCF between the fiber capillaries.

3. Computational study

There are a variety of computational techniques for modeling modes and solving scattering problems associated with MOFs. These include purely numerical techniques, such as the finite element method (FEM), and semi-analytic techniques such as the multipole method. Indeed, a recent study of writing a fiber Bragg grating in the doped, photosensitive core of a MOF [5] referred to a 2D FEM simulation of the transverse scattering of a plane wave by a MOF. This contrasts with our modeling, in which we chose a semi-analytic treatment (for the reasons given below) to study the scattering of a Gaussian beam by the microstructured cladding, in order to realistically model the actual delivery of power to the core.

The modeling challenges are quite formidable in problems of this type since the structure is very large in comparison with the wavelength, which is also small in comparison with the size of individual scatterers. For the structure that we are considering, the computational domain is approximately $60\,\mu m \times 60\,\mu m$ while the wavelength within the (glass) cladding region is $\lambda_c = 267nm/1.5 = 178nm$. Typically, when using a conventional numerical tool such as a finite element or finite difference method, one would require (approximately) 10 mesh points per wavelength in order to achieve a well converged solution, and so the computational domain would need to be spanned by (of the order of) 10^7 mesh points—an extremely large number. To put this in context, we are seeking to solve an electromagnetic optics scattering problem, the scale size of which is approaching the limit at which the laws of geometrical optics may be applicable.

Given our desire to model the transverse scattering problem on a desktop workstation in a reasonable time, we elected to use a semi-analytic method which takes advantage of the geometry, and so we were led to the multipole method that allowed us to develop a solver that is both efficient and compact. The treatment that we adopt is based on the foundations of a multipole method [13, 14], developed originally for the calculation of leaky modes in microstructured optical fibers (MOFs). Our modeling provides for the solution of both in-plane (2D) and conical incidence (2.5D) problems. For brevity, however, we outline the formulation only for the 2D in-plane problem, with the generalization to 2.5D following in a straightforward manner.

We consider a jacket, inside which the air holes are arranged in some pattern, and outside which there is a source located in an infinite medium. The field outside of the jacket can be expressed in the form

$$V(r) = V_G(r) + \sum_{n=-\infty}^{\infty} B_n^0 H_n(kv_e \mid r - r_0 \mid) e^{in\arg(r-r_0)}, \tag{1}$$

where $V_G(r)$ is an incident Gaussian beam represented by

$$V_G(r) = \frac{W}{2\sqrt{\pi}} \int_{-\infty}^{\infty} e^{-(\alpha-\alpha_0)^2 W^2/4} e^{i\alpha x + i\sqrt{k^2 v_e^2 - \alpha^2} y} \, d\alpha, \tag{2}$$

and where v_e is the refractive index outside the jacket, W denotes the width of the Gaussian beam, r_0 is the position of the centre of the jacket, $k = 2\pi/\lambda$ is the free space wavenumber, and $\alpha_0 = kv_e \sin\theta_i$, where θ_i is the angle of incidence of the beam.

Inside the jacket, in the microstructured cladding region, which has refractive index v_c, the field is expressed as a Wijngaard expansion:

$$V(r) = \sum_{l=1}^{N_c} \sum_{n=-\infty}^{\infty} B_n^l H_n^{(1)}(kv_c \mid r - r_l \mid) e^{in\arg(r-r_l)} + \sum_{n=-\infty}^{\infty} A_n^0 J_n(kv_c \mid r - r_0 \mid) e^{in\arg(r-r_0)}, \tag{3}$$

in which J_n denotes a Bessel function of the first kind, and $H_n^{(1)}$ is the order n Hankel function of the first kind. In Eq. (3), the first term represents outgoing waves sourced on each cylinder l, which is centered on r_l, and the second term represents the standing wave field that is sourced at the cladding boundary, and which is incident on each of the cylinders. Within each cylinder, in which the refractive index is taken to be v_i, the field is represented by

$$V(r) = \sum_{n=-\infty}^{\infty} C_n^l J_n(kv_i \mid r - r_l \mid) e^{in\arg(r-r_l)}. \tag{4}$$

We now form the key field identity that encapsulates the multiple scattering processes that occur within the cladding. In the near vicinity of cylinder l, the field is represented in a local expansion which comprises outgoing waves from that cylinder (given by the lth term of the first expression in Eq. (3) and the regular part of the local field about cylinder l, which has the form $\sum_n A_n^l J_n(kv_c \mid r - r_l \mid) e^{in\arg(r-r_l)}$. This regular part is due to outward radiation from all other scatterers and also the jacket boundary—a physical construct that leads to the field equation. Combining all of the equations in a matrix notation and denoting by $A = [A^l]$, a partitioned vector of multipole coefficients $[A_n^l]$, and similarly for $B = [B^l]$, we can write $A = HB + J^{L0} A^0$, in which the first term HB denotes the outward radiation from the other cylinders and $J^{L0} A^0$ represents the incoming radiation sourced at the jacket boundary. Here, H and J^{L0} perform the necessary changes of basis from the coordinate system of one scattering centre to another, with H denoting a block partitioned matrix $H = [H_{nm}^{lj}]$, the entries of which follow from applications of Graf's Theorem and are given by $H_{nm}^{lj} = H_{n-m}^{(1)}(kv_c \mid r_j - r_l \mid) e^{-i(n-m)\arg(r_l-r_j)}$. Similarly, $J^{L0} = [J_{nm}^{l0}]$ expresses the change of basis from the global (jacket) coordinate system to the local coordinate system of each scatterer, with $J_{nm}^{l0} = J_{n-m}(kv_c \mid r_l \mid) e^{i(n-m)\arg(r_l)}$.

The outgoing fields from each of the cylinders that comprise the MOF cladding are represented by B and may be regarded as reflections of the incoming fields A, i.e. $B = RA$, while the fields interior to each scatterer C may be thought of as a transmission of the incident field, i.e., $C = TA$. Here, R and T are multipole scattering matrices, the exact forms for which are given in Refs. [12,13]. Correspondingly, the field sourced at the interior of the jacket is $A^0 = \hat{R}' B^0 + \hat{T} Q$, i.e. a reflection ($\hat{R}'$) of the sum of all outgoing fields

within the cladding ($B^{0} = J^{0L}B$) and a transmission ($\hat{T}$) of the exterior Gaussian beam sources (Q). Here, $J^{0L} = \left[J^{0l}_{nm}\right]$, with $J^{0l}_{nm} = J_{n-m}(kv_{c}\,|r_{l}\,|)e^{-i(n-m)\arg r_{l}}$, performs a change of basis from the local coordinate systems of the scatterers to the global (jacket) system, while the Gaussian beam source, in the region exterior to the cladding boundary, is expressed by the multipole expansion $\sum_{n}Q_{n}J_{n}\left(kv_{e}\,|r-r_{0}|\right)e^{in\arg(r-r_{0})}$. In the case considered here, we model the source by a Gaussian beam of half width $W = 4\,\mu$m and then express this in the global coordinate system to obtain the source coefficients $Q = \left[Q^{l}_{n}\right]$ according to

$$Q^{l}_{n} = \frac{i^{n}W}{2\sqrt{\pi}\left(kv_{e}\right)^{n}}\int_{-\infty}^{\infty}e^{-(\alpha-\alpha_{0})^{2}W^{2}/4}e^{i\alpha x_{l}+i\sqrt{k^{2}v_{e}^{2}-\alpha^{2}}y_{l}}\left(\alpha - i\sqrt{k^{2}v_{e}^{2}-\alpha^{2}}\right)^{n}d\alpha. \tag{5}$$

Combining all of these expressions, we derive a system of linear equations for the multipole coefficients B from which the field can be reconstructed everywhere:

$$B = \left(I - RH - RJ^{L0}\hat{R}'J^{0L}\right)^{-1}RJ^{L0}\hat{T}Q. \tag{6}$$

While the derivation outlined here has been for the 2D treatment, the method extends naturally to 2.5D, with the fields becoming entirely vectorial. We note also that while this derivation has solved the transverse scattering problem, the calculation of the leaky modes of a MOF can be inferred directly from Eq. (6) by noting that a mode is simply a non-trivial solution of the field problem in the absence of a driving field. The eigenvalue problem for the modes thus requires the scattering matrix to be singular, i.e., $\det\left(I - RH - RJ^{L0}\hat{R}'J^{0L}\right) = 0$, the complex solutions of which give the propagation constants β of the leaky modes.

Our convergence studies have shown that for a wavelength of $\lambda = 267$nm, a minimum of 151 terms (i.e., including harmonics $n = -75, ..., 0, ...75$) in the multipole series is needed to achieve an accuracy of 4 significant figures. In the examples considered in this paper, there are of the order of 9,000 unknowns in the linear Eq. (6), and this in turn requires that the code be implemented carefully, with numerous programming optimizations and also exploiting efficient libraries in order to achieve accurate results in a reasonable time.

4. Experimental and computational results

The experimental and computational model results for TE polarization (transverse electric field with the magnetic field oriented along the fiber axis, i.e.: the native vertical polarization of the laser intersecting the horizontally held PCF) are shown in Fig. 3. The experimental data are presented at 1° increments, and for clarity are plotted over a reduced angle range of 160°. The experimental and computational data are in excellent agreement showing the same functional form and exhibit a 60° repeating interval with 30° reflections about the interval centre, given the symmetry of the hexagonal cladding lattice.
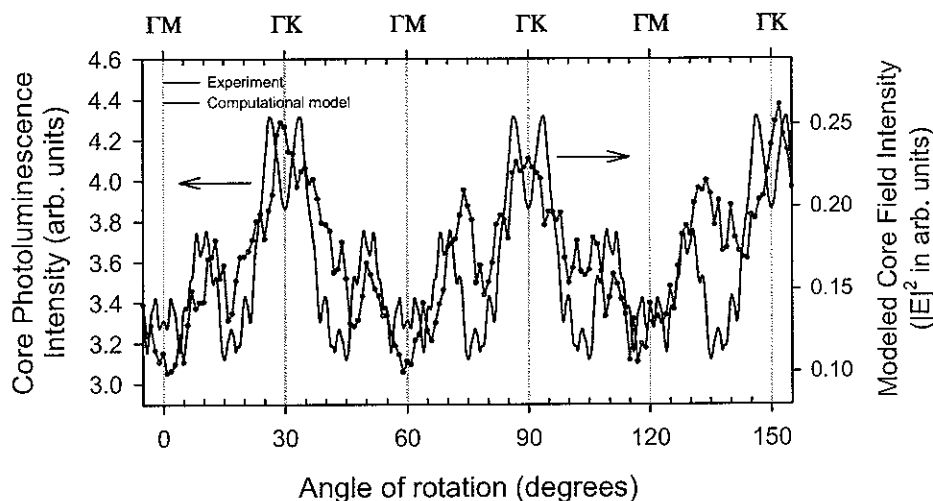
Fig. 3. TE polarization PCF core photoluminescence intensity and computational model whole-core field intensity as a function of PCF rotation angle.

The angles 30°, 90° etc. correspond to the trajectory at which light is incident on an apex of the core's hexagonal form, as defined by the surrounding lattice, i.e. the ΓK direction. (The angles 0°, 60° etc. correspond to the ΓM direction.) The peak in the transverse-coupling to the fiber core occurs approximately 4° from the angle of 30° (at angles 26° and 34°) and all subsequent rotations of 60°. Near identical experimental and modeling results to those presented in Fig. 3 are obtained when the polarization of the incident light is parallel to the fiber axis (transverse magnetic field or TM polarization). In the TM case, the modeled maximum transverse-coupled core field is marginally (2.5%) higher whilst the minimum remains virtually identical. The modeled all-angles averaged transverse-coupled core field is slightly higher (1.2%) in the TE case. A comparison of the modeled TE and TM data is presented in Fig. 8. Considering all of the very marginal differences between the two orthogonal polarization states predicted by the computational model, there is no experimental advantage in using one polarization state over the other to couple light into the fiber core.

So that the computational model may accurately represent the manner in which the experimental photoluminescence is generated, the core field intensity is summed over all 10186 voxels that comprise the core region. By studying just the centre region of the fiber core yields intensity vs. angle data that are significantly different to those presented in Fig. 3. For example, the data presented in Fig. 4 illustrate that the angle of peak transverse coupling, with the intensity averaged over one tenth of the core area, is predicted at approximately 9° and 51°, while taking into account only the centre voxel yields maxima at 11° and 49°. This is in contrast to the whole core averaged data that peak at 26° and 34°, shown in the blue curves of Fig. 3 and Fig. 4.
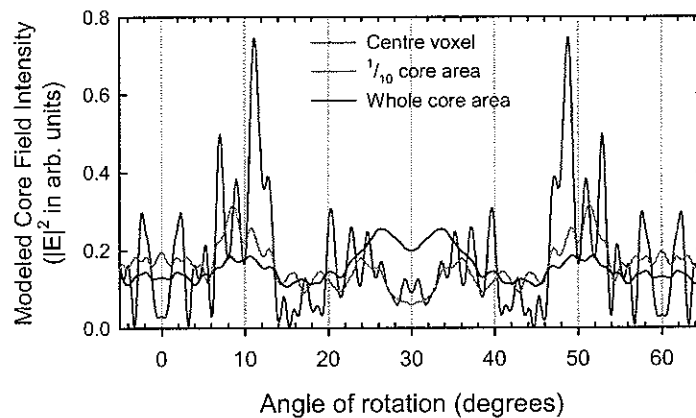
Fig. 4. The modeled TE core field intensity as a function of angle. The different curves represent the field intensity averaged over the whole core area, one tenth of the area and the centre voxel only. Note that the blue curve here is the same as that in Fig. 3.

The raw intensity data used to generate Fig. 3 and Fig. 4 are displayed in the animation associated with Fig. 5 (available in the online version). Fig. 5 (paper version) shows two stills from the animation for the angles $\theta = 26°$ and $\theta = 15°$, respectively corresponding to the maximum and minimum averaged (over the entire core region) intensity that can be delivered to the core. Fig. 5 demonstrates that in order to deliver the maximum intensity to the PCF core, it is important to minimize scattering by the air holes. This figure also reveals that in the short wavelength limit, the process of geometrical scattering dominates the interaction of the incident light within the photonic crystal lattice. Accordingly, we deduce that an optimal incidence angle can be found geometrically by constructing a line that joins the exterior of the cladding to the center of the core, avoiding wherever possible any intersection with an air hole. We note that the angle for optimal coupling to the core appears to lie approximately in the ΓK direction; minimal coupling is approximately associated with the ΓM direction.
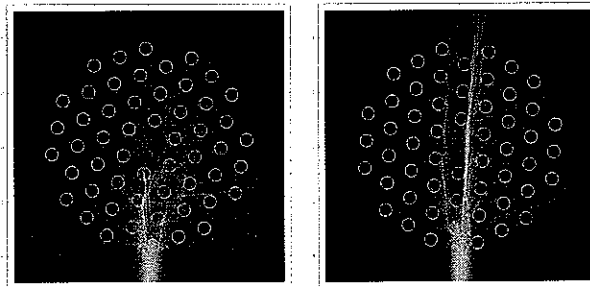

Fig. 5. (2.57 MB) Two stills taken from a single movie of the effect of PCF rotation angle on transverse-coupling at 267 nm. The still on the left shows the case of poorest coupling to the core; the still on the right shows optimal coupling to the core. The incident light is linearly polarized in the TE direction and the scale is in units of the lattice spacing i.e. one unit represents 8.0 μm.

While the interaction of the PC lattice with the light is dominated by geometrical scattering at this wavelength (267 nm), the lattice does not completely prevent transverse coupling to the fiber core. In the experimental case, approximately 70% of the maximum PL signal is present at the poorest coupling angle while, in the modeling, this corresponded to a core field intensity of 42%. This discrepancy is most likely to be due to imperfections in the

experimental setup, and also to the non-linear nature of the PL signal generation due to the incident light field. We also note that the presence of light in the core of the fiber can be seen at all angles of incidence. At the angle of greatest coupling efficiency into the core, one effect of the scattering centers is to locally enhance the field strength to a value above the strength in the incident beam. Furthermore one can observe that a portion of the incident beam scatters through the complete microstructured region. This through-scattered light was observed during the experimental procedure and, since it is present only at angles close to the optimum for transverse-coupling, it can provide a useful means for determining the angle of fiber rotation if the hexagonal lattice is not visible.

In the modeling results presented so far, the incoming beam waist of 4.0 µm half-width was selected to be the same as that in the experimental case. However, it does not necessarily follow that this is the optimum waist for the purpose of transverse coupling. In a modeling study of the effect of waist size on the efficiency of transverse coupling it was found that using a waist of 8.0 µm half-width resulted in slightly poorer coupling, whereas using waist of 2.0 µm half-width resulted in approximately the same coupling efficiency as in the 4.0 µm case. In all cases, the effect of fiber rotation was found to similar with the peak in coupling occurring between 26 to 28°.

5. Further computational results

Given the success of the computational model in predicting the transverse-coupling of the incident light field with fiber rotation, the same model was used in several further studies. The first analyzed the effect of fiber translation where the optical fiber was moved laterally with respect to the incident light field. This was conducted at three fixed rotational angles; those that gave the most and least efficient transverse-coupling (26.3° and 15.0° respectively), and 30°, i.e. the ΓK direction. The second study repeated the initial rotational study, but this time for 800 nm light of TE and TM linear polarizations. Finally, the effect of increasing the scattering hole diameter was qualitatively investigated (up to the limit where the holes completely obscure any direct line of sight to the fiber core). This latter study revealed that the efficiency of transverse coupling decreases monotonically with increasing hole diameter while the angle of optimal coupling remains approximately constant.

The results of the lateral shift study are shown in Fig. 6. The lateral shift is presented in units of the PCF lattice spacing (or hole pitch), which is 8.0 µm. In the 30.0°, plot the data are symmetric about the center (zero shift) position, as would be expected considering the symmetric nature of the fiber and beam geometry. In all the rotational angles studied the peak of transverse-coupling lies away from the zero shift position. In the 26.3° case, a 14% increase in the transverse-coupling can be achieved when the lateral shift ($\delta x / d$) is 0.22 or 1.8 µm from the center position. While this point represents the highest modeled transverse-coupling efficiency, it does not necessarily follow that this is the optimal choice. A parametric study would be required to reveal the optimum combination of angle and lateral shift.
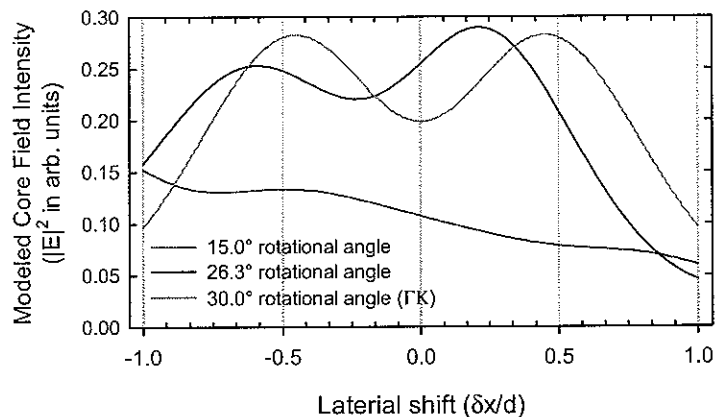
Fig. 6. Modeled coupling to the fiber core with lateral shift for three angles of incidence. The angles of 26.3° and 15.0° respectively give maximum and minimum transverse-coupling efficiency to the core in the rotation study. The 30.0° case exhibits exact symmetry about the center point.

The model data used to generate Fig. 6 have been compiled into two animations (available in the online version) that visualize the scattering processes during lateral translation. Two stills presenting the modeled lateral shifts that give maximum transverse-coupling are presented in Figs. 7(a) and 7(b) for the 15.0° and 26.3° cases respectively. In the 15.0° case, the transverse-coupling is seen to decrease monotonically with increasing lateral shift (within the modeled lateral shift range of $\delta x/d = \pm 1.00$).

(a)   (b)
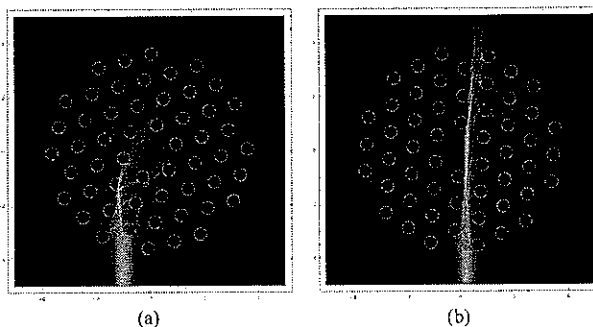
Figs. 7. (a). and 7. (b). (1.13 MB & 1.16 MB) Movie stills of the positions of greatest transverse-coupling taken from two animations showing the effect of beam translation on transverse-coupling with a lattice angle of (a) 15.0° and (b) 26.3°. The lateral shifts are (a) $\delta x/d = 1.00$ and (b) $\delta x/d = 0.22$. The incident light is linearly polarized in the TE direction and the scale is in units of the lattice spacing.

Recently, the 800 nm wavelength output of a femtosecond laser was used to inscribe Bragg gratings in PCFs [9]. Our computational model can be applied easily to this wavelength and the results of a rotational angle study at 800 nm are presented in Fig. 8. For comparison, the two different linear polarizations at 267 nm and 800 nm are plotted along side each other in Fig. 8. The maximum and minimum transverse-coupling angles for 800 nm TE polarization are 25.2° and 15.8° respectively.
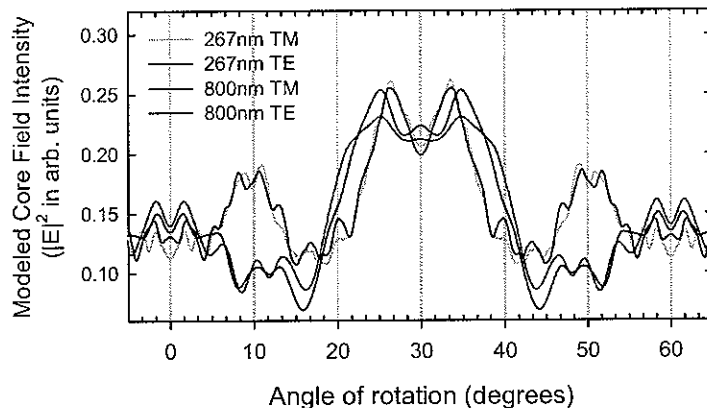
Fig. 8. Modeled transverse-coupling efficiency for 267 nm and 800 nm radiation in both TE and TM polarizations. The 267 nm TE data presented here are the same as those shown in Fig. 3.

The data used to generate the plots of Fig. 8 are presented in an animation (online version) in Fig. 9. It is interesting to note that although the 267 nm and 800 nm cases presented in Fig. 8 display approximately the same overall form (with a peak around ΓK), the animation of Fig. 9 reveals that diffraction effects are now evident. This is despite the wavelength being short in comparison with the feature size of the PCF, and is in contrast to the $\lambda = 267$ nm case, in which the propagation was governed essentially by ray optics.
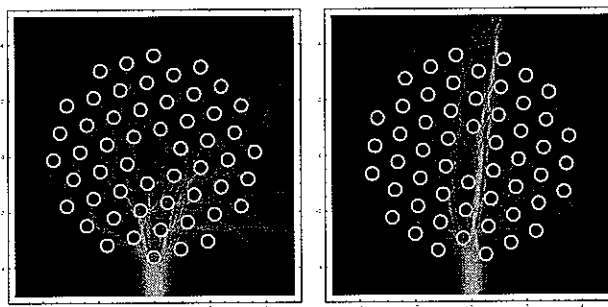

Fig. 9. (2.11 MB) Two stills taken from a single movie of the effect of PCF rotation angle on transverse-coupling at 800 nm. The still on the left shows the case of poorest coupling to the core; the still on the right shows optimal coupling to the core. The incident light is linearly polarized in the TE direction and the scale is in units of the lattice spacing i.e. one unit represents 8.0 μm.

6. Conclusions

By combining experimental and computational modeling results, we have quantified the scattering effect of the air hole structures in a PCF and revealed the effects of fiber rotation and lateral translation at two wavelengths used to inscribe gratings in PCF. It is clear from this study that the microstructured region does not completely obstruct transverse optical paths to the core even when the angle of alignment is at its poorest. Notably, there is significant variation in the transverse-coupling efficiency to the fiber core with angle and lateral position which, if not controlled, will have the effect of creating a variation in the rate

of Bragg grating growth rate between samples of PCF. There is little dependence of transverse-coupling on the state of laser beam polarization due to the fact that the scattering processes are dominated by relatively large body interactions (i.e. geometric optics processes where $\lambda / d \ll 1$). For this same reason, the effect of the air-hole lattice on the incoming light field is dominated by scattering processes and not resonant or band gap effects. Nevertheless, we note that since our model provides a rigorous solution of Maxwell's equations, band gap phenomena, should they exist, would be characterized completely by our model.

The observation of through scattered light at angles close to the optimal rotation angle for transverse-coupling provides a useful means for determining the angle of the optical fiber with respect to the incident light. This is particularly useful to grating writing processes when the orientation of the hexagonal lattice of air holes is not directly visible, as is common when working with continuous lengths of fiber.

The efficiency of transverse coupling at 267 nm and 800 nm is approximately the same and both wavelengths have optimal angles of fiber approach around the ΓK direction, although the rate of grating growth at these two different wavelengths will differ significantly. The UV and IR radiation photochemical processes that lead to refractive index modification in pure fused silica have different thresholds and growth rates [15].

In this work we have studied one commonly used design of PCF and our modeling technique is equally applicable to other designs of fiber that incorporate circular air holes. Further studies of fibers with different hole geometries could be made for the purpose of improving grating writing efficiencies. A study of a range of fibers may also elucidate more wide ranging conclusions regarding techniques for grating manufacture in PCFs.

The geometry considered herein is a purely 2D transverse one. In a phase mask Bragg grating writing geometry, the additional effect of "out-of-plane" beam propagation and wavefront phase becomes an important consideration since it is the interference between two copies of the writing beam that generate the fringes and, in turn, the Bragg grating in the fiber. The computational model used in this study is well suited to an extension into this third dimension (thereby creating a 2.5D system) and indeed this exciting and challenging problem is an ongoing topic of our investigations.

Acknowledgments